# RF-Powered Variable Duty Cycle Wireless Sensor

Daniel Costinett, Erez Falkenstein, Regan Zane, Zoya Popovic

*Department of Electrical, Computer and Energy Engineering*
*University of Colorado*
*Boulder, CO 80309, U.S.A.*

regan.zane@colorado.edu
zoya@colorado.edu

***Abstract*— This paper discusses a low-power 2.4GHz ISM band wireless sensor based on commercial components for sensing and data transmission. The sensor is powered wirelessly in the 5.8-GHz ISM band through an integrated dual-polarization antenna, rectifier and power management module. Since the unit is intended for mobile use, the variable available power is monitored, and the duty cycle for wireless data transmission adaptively adjusted through use of a low-power microcontroller and a custom power management circuit. In sleep mode, the circuit consumes 1μA at 2.5V.**

## I. Introduction

In many electronic applications running wires to a device or changing/charging batteries is either not possible or is associated with maintenance difficulties. Some examples associated with wireless sensing are implanted sensors for medical diagnostics and therapy, sensors inside hazardous manufacturing or other hazardous environments, sensors for health monitoring of patients [1], aircraft health monitoring [2,3], sensors for covert operations, etc.

The concept of wireless power transmission via far-field RF radiation has been considered since the beginning of the 20th century [4]. Wireless powering can be differentiated into near- and far-field. In the near-field case, the powering device is small compared to the wavelength and is inductively (or capacitively) coupled to the source, making it sensitive to its relative position [5,6]. Far-field directive beaming with high power densities has been the topic of research over the past few decades for various applications, e.g. [7]-[9]. Far-field powering implies plane wave propagation between antennae at longer range, can be done without line of sight, and is less sensitive to the orientation and position relative to the transmitting antenna. Few applications have taken advantage of this technology for harvesting energy at sub-milliwatt power levels attributed to the challenges associated with optimizing the interface between the power reception device, and typical low-power sensor loads to achieve high overall efficiency [10, 11].

The work in this paper addresses far-field powering at low incident power densities (below 150μW/cm$^2$). It differs from radio frequency identification (RFID) devices in that the powering is independent of signal transmission and is done at different time scales, power levels and frequencies.

A block diagram for the prototype described in this work is shown in Figure 1. An antenna integrated with a rectifier receives arbitrarily polarized radiation at 5.8GHz at levels at or below 125μW/cm$^2$. The DC output is managed by a digitally controlled power converter in such a way that it always presents an optimal DC load to the energy storage device, which provides power to the microcontroller, sensor and data transceiver. The sensor data is input to a commercial low-power wireless transceiver operating in the 2.4GHz ISM band. The data transmission is the most power-consuming task and is not done continuously, which is acceptable for most applications. If there is not enough stored energy, the data cannot be transmitted and there is danger of damaging the storage device. Therefore, the available rectified RF power and the available energy stored are monitored in a closed-loop system allowing for adaptive adjustment of the data transmission duty cycle.

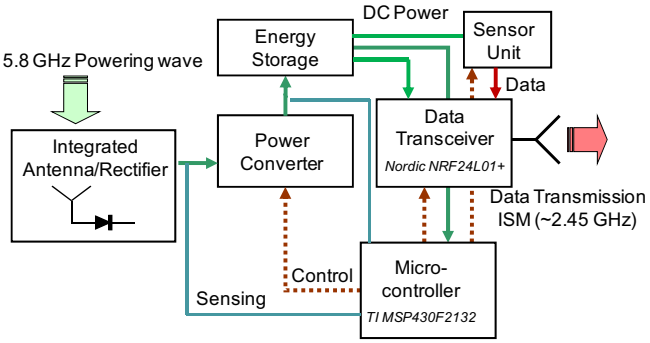


Fig. 1. Block diagram of far-field RF-powered wireless sensor. The available rectified RF power and the available energy stored are monitored (shown in light blue lines) allowing for adaptive adjustment of the data transmission duty cycle. The low-power microcontroller provides control to the power management circuit, wireless transceiver and sensor. The power is collected in the far field of one or more ISM transmitters at 5.8GHz, independently of data transmission.

In the remainder of the paper, the details of the power receiving integrated antenna/rectifier are discussed, followed by a discussion of the power management circuit. The paper concludes with measured power consumption and timing diagram of the entire wireless sensor platform.

## II. RF Power Reception

An integrated antenna/rectifier (often termed "rectenna") is designed to receive arbitrary polarized 5.8GHz radiation at

low incident power densities. Rectennas for 5.8GHz reception have been demonstrated earlier with high RF-DC conversion efficiency, e.g. [12], but for significantly higher incident power densities and with linear polarization. In an unknown multipath environment, the polarization is random, and it has been shown that rectifying two orthogonal polarizations independently and adding the resulting DC power increases overall efficiency [13,1]. A photograph of a dual-linearly polarized patch antenna used in this work is shown in Figure 2. Two Skyworks Schottky diodes are connected to the centres of the radiating edges at the high-impedance points. Each diode rectifies power received in one polarization, and is in the voltage null for the orthogonal polarization, providing polarization diversity. The antenna is simulated using both HFSS and Agilent Momentum, with good agreement.

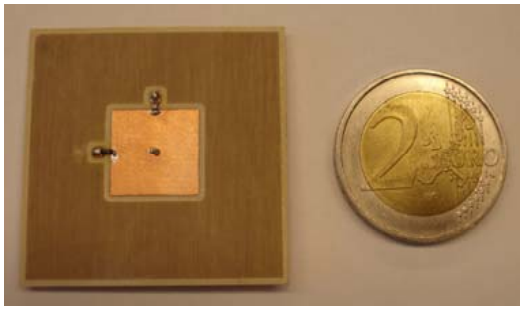

Fig. 2. Photo of integrated antenna/rectifier for 5.8GHz dual polarization reception and rectification. The antenna is fabricated on a Rogers 4350b substrate, and the diodes are soldered to the high-impedance points. The two DC connections are taken from the diode terminals and through an isolated via in the voltage null of the patch, which is 1.3mm squared in size.

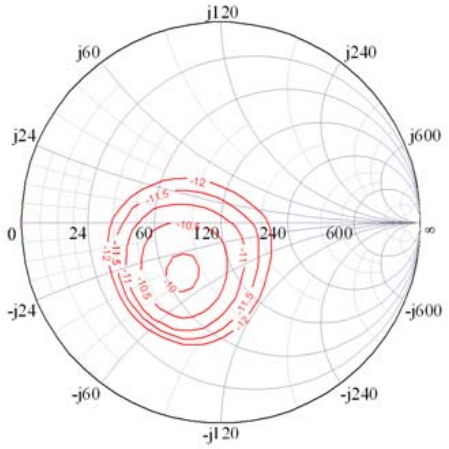


Fig. 3. Source pull contours for the Skyworks Schottky diode at 5.8GHz, showing contours of constant rectified power in dBm. The incident power is 0dBm and the DC load is 100 Ω for this measurement, and the Smith chart is normalized to 120 Ω.

Notice that there are no matching circuits between the antenna feed points and the diodes, for simplicity and small size. In order to determine the optimal diode impedance for rectification, a Focus Microwave load-pull system is used in a modified source-pull RF to DC configuration. Calibration standards bring the reference plane to the diode, and the input power is varied while directly measuring DC power into a variable DC load. The results of these measurements are impedance contours of rectified power. Since the range of possible parameters is large, we here show only one sample plot for the Skyworks SMS7630-79 diode, with 0dBm incident power, a DC load of 100 Ω at 5.8GHz. This data can be also confirmed with harmonic balance simulations [13].

From several measurements over input power, DC load and frequency, the RF impedance for best average rectification over the variables can be determined. In this case it was an impedance with a real part between 60 and 115Ω, with a small imaginary capacitive component which is easily compensated with diode lead inductances and via to ground.

The testing of the antenna/rectifier is performed in an anechoic chamber over a variety of incident power levels (from 25 to 125 μW/cm$^2$) and the rectified power is plotted as a function of the DC load. Figure 4 shows the results for orthogonally polarized incident waves.

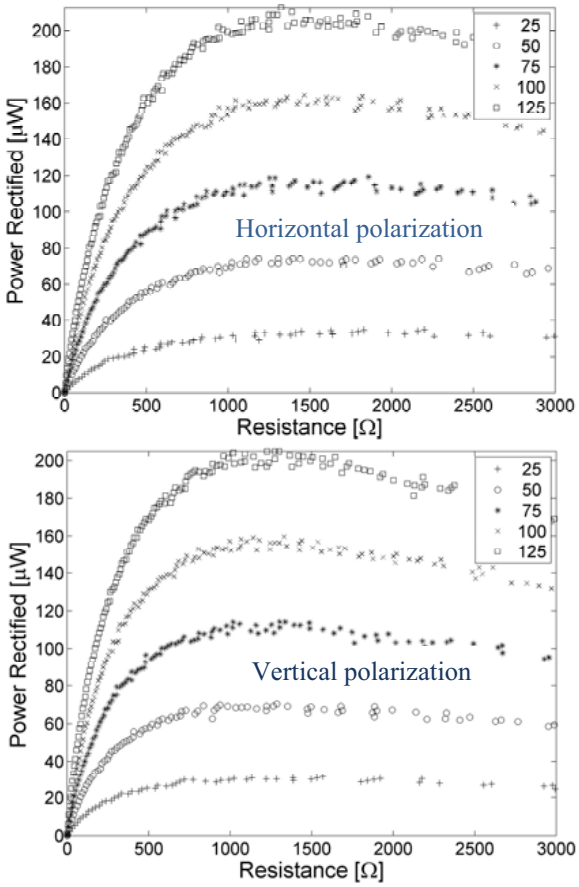


Fig. 4. Measured DC rectified power as a function of DC load for various power densities (in μW/cm$^2$) when the normally incident wave is linearly polarized and co-polarized with each of the patch edges. The best DC load resistance is around 1000 Ω in each case and is roughly the same for the entire power range.

From the plots in Fig.4, it can be seen that:

- The response to incident waves in the two orthogonal polarizations is almost identical, indicating good polarization isolation;

- The best DC load resistance in all cases is around 1000Ω, which means that the converter circuit in the power management unit in Fig. 1 should be designed to emulate a resistance in this range;
- The DC-RF conversion efficiencies can be estimated by assuming the entire area of the rectenna $A$ is the effective area, giving an underestimate for the efficiency. The peak efficiency for the tested range of power densities $S$ is larger than 18%:

$$\eta_{RF-DC} = \frac{P_{DC}}{A \cdot S_{RF}} \approx 0.18$$

## III. Power Management

Referring to the block diagram in Fig. 1, the power management circuit consists of a micro-controlled DC-DC converter which optimally charges a Seiko MS412FE battery. The converter topology, shown in Fig. 4, is an asynchronous DCM boost converter where the MOSFET gate drive signal is a buffered output from the Texas Instruments MSP430F2132 low-power microcontroller. The gate drive signal has both a high-frequency period and duty cycle, $T_{HF}$ and $D$, and a low-frequency period and duty cycle, $T_{LF}$ and $k$, which are altered in order to match the converter emulated resistance to the optimal DC resistance of the integrated antenna/rectifier [14]. The high-frequency component is supplied by the MSP430's internal oscillator and ranges from 100kHz to 1MHz at a fixed duty cycle $D$=0.5. The low frequency component is sourced from the internal very low-power, low-frequency oscillator (VLO) which operates at a nominal frequency of 12kHz. Both clock sources are then fed into on-chip timers to allow control over $T_{LF}$ and $k$ as well as regulate the output state of the high frequency component when the DCO is turned off.

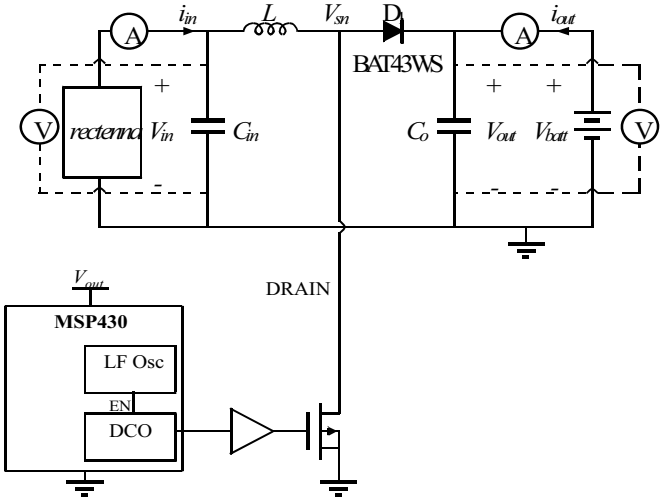


Fig. 5. Circuit diagram of the converter portion of the power management module. The rectenna is represented as an equivalent Thevenin source obtained from the measured curves in Fig. 4.

If the device is not actively sensing or transmitting, the processor is allowed to go into a sleep mode, waking only briefly on the rising and falling edges of the low-frequency interval.

Adaptive transmission uses predefined limits in a lookup table to determine the duty cycle of the wireless transceiver, which is in sleep mode between data transmissions. For the data presented here, transmission frequency, $f_{trans}$, occurs at three discrete intervals corresponding to about 20, 1.5, and 0.4Hz transmission frequencies, determined by the on-chip "watch-dog" timer. The lookup table itself is constructed so that the average energy of each transmission is

$$W_{trans} = \int i_{trans} V_{batt} \approx 20.5\ \mu J,$$

where $i_{trans}$ is the transceiver current shown in Fig. 7. Input power is determined by sampling the input voltage and operating a known emulated resistance given by the measured data in Fig. 4. Then, given the measured efficiency of the converter, conservative limits are set to ensure that the frequency of transmission consumes significantly less power than will be harvested:

$$P_{harv} = \eta_{DC-DC}(V_g^2 / R_{em}) < W_{trans} f_{trans}$$

A battery monitoring routine checks the battery voltage to determine the state of charge and can enable/disable both transmission and the boost converter if the battery is at risk of overcharging or discharging completely. For battery voltage below 2.2V (90% discharged), all transmission is disabled and the converter is disabled if the input power is below 25µW. For battery voltage above 2.85V, the converter is shut down so that no further power is sent to the battery and transmission is allowed to continue at the highest duty cycle until the battery voltage drops below 2.8V. If the battery voltage is between 2.7 and 2.3V, the frequency with which the battery is monitored is reduced from once every 10 transmission duty cycles to once every 20 cycles. The efficiency of the power management circuit is measured directly with a very small, high resistance inductor, and the results are shown in Fig. 6. The storage element operates at a nominal voltage of about 2.5V, so all power numbers are given at a 2.5V supply. This efficiency does not take into account the rectenna efficiency, which is a function of incident power density and polarization.

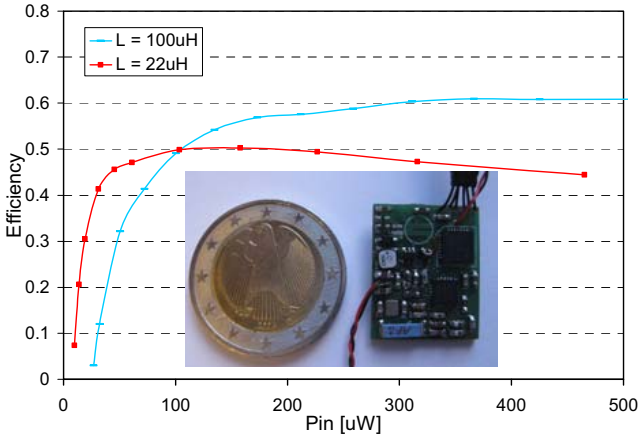


Fig. 6. Measured efficiency of circuit as a function of available input DC power for two choices of inductance value, L. The 2.1x1.7cm circuit contains both power management and sensor/transmitter circuitry.

## IV. Discussion

The wirelessly transmitted data in this implementation samples input and output voltages of the converter (Fig.1) and an on-chip temperature sensor, integrated into the MSP430F2132. However, the design is fully capable of handling more external sensors with available A-to-D converter pins and this is the topic of current work. The transmission current diagram is shown in Fig. 7, with a sleep current of less than 1μA at 2.5 V. The wireless sensor platform is capable of transmitting bursts of 2Mbps of data with less than 8mA.

When the entire sensor is tested in an anechoic chamber with varying levels of incident power density, the results shown in Table I were measured. As the RF power is decreased, the frequency of transmission adaptively decreases.

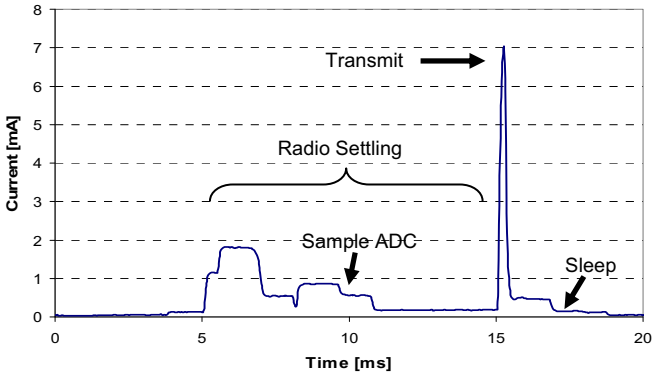


Fig. 7. Measured total current consumption of the circuit described in Fig. 1 and shown in Fig. 6.

TABLE I
ADAPTIVE TRANSMISSION TEST RESULTS USING PATCH ANTENNA OF FIG. 2. NEGATIVE $I_{OUT}$ INDICATES NET POWER FLOW INTO THE BATTERY.

| $V_{batt}$ [V] | RF Power Density [μW/cm$^2$] | $V_g$ [V] | Avg $f_{trans}$ [Hz] | $I_{out}$ [μA] |
|---|---|---|---|---|
| 2.5 | 150 | 0.826 | 5.0 | -63.1 |
| 2.5 | 105 | 0.697 | 1.5 | -57.2 |
| 2.5 | 50 | 0.505 | 1.5 | -23.4 |
| 2.5 | 30 | 0.342 | 0.4 | -10 |
| 2.5 | 12.5 | 0.182 | -- | -0.4 |
| 3 | 50 | 0.801 | 20 | 132 |
| 2 | 50 | 0.501 | -- | -43.5 |

The rectenna can also be made on a flexible substrate without a metal ground plane, and the potential of the circuit designed as a CMOS chip [15] and integrated in the slot ground. Fig. 8 shows an implemented folded slot antenna prototype with a roughly 100-Ω input impedance and the measured data for both linear polarizations.

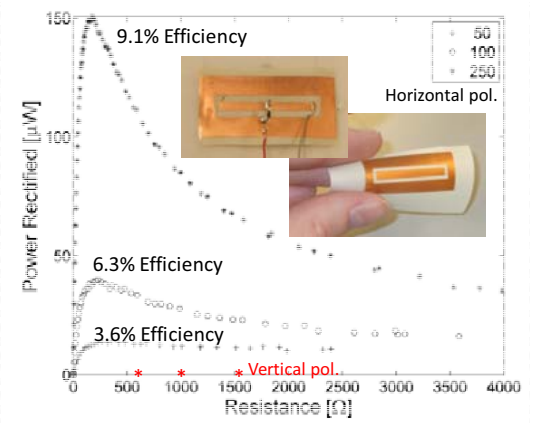


Fig. 8. Measured rectified power at 5.8GHz with a folded slot rectenna on a flexible substrate. The slot is linearly polarizaed and the cross-polarized rectified power is shown in red.

## Acknowledgment

This work was funded by the Colorado Power Electronics Cener (CoPEC) Northrop Grumman directed project, and the National Science Foundation under a collaborative grant, ECCS-0701780. Profs. Regan Zane and Zoya Popovic acknowledge support of the Coleman Foundation through Coleman Faculty Fellowship sabbatical awards.

## References

[1] T. Paing, A. Dolgov, J. Shin, J. Morroni, J. Brannan, R. Zane, Z. Popovic, "Wirelessly powered wireless sensor platform," 2007 *European Microwave Conf. Digest*, pp. 241-244, Munich, Oct. 2007.

[2] C. Walsh, S. Rondineau, M. Jankovic, G. Zhao, Z. Popovic, "A Conformal 10-GHz Rectenna for Wireless Powering of Piezoelectric Sensor Electronics," *IEEE 2005 IMS Digest,* Long Beach, June '05.

[3] X. Zhao, T. Qian, G. Mei, C. Kwan, R. Zane, C. Walsh, T. Paing, Z. Popovic, "Active health monitoring of an aircraft wing with an embedded piezoelectric sensor/actuator network," *Smart Materials and Structures,* 16(2007), pp. 1218-1225, June 2007.

[4] Jim Glenn, Ed., *The Complete Patents of Nikola Tesla,* Barnes and Noble Books, New York, 1994, pp. 346-360.

[5] B. Jiang, J. Smith, M. Philipose, S. Roy, K. Sundara-Rajan, and A. Mamishev, "Energy scavenging for inductively coupled passive RFID systems," in *Proc. IEEE Instrumen. Meas. Technol. Conf., IMTC 2005*, May 16–19, 2005, vol. 2, pp. 984–989.

[6] A. Kurs, A. Karalis, R. Moffatt, J.D. Joannopoulos, P. Fisher, M. Soljacic, "Wireless Power Transfer via Strongly Coupled Magnetic Fields," *Science,* Vol. 317 no. 5834, 2007, pp. 83-86. Also published online on 7 June 2007 (10.1126/science.1143254).

[7] W.C. Brown, "The history of power transmission by radio waves," *IEEE Trans.Microw.Theory Techn.*, vol. 32, pp. 1230–1242, Sept. 1984.

[8] J.C.Lin, "Space solar-power stations, wireless power transmissions, biological implications," *IEEE Microw. Mag.*, pp. 36–42, Mar. 2002.

[9] J. O. McSpadden, F. E. Little, M. B. Duke, and A. Ignatiev, "An in-space wireless energy transmission experiment," in *Proc. IECEC Energy Conversion Eng. Conf.*, Aug. 1996, vol. 1, pp. 468–473.

[10] T. Le, K. Mayaram, and T. Fiez, "Efficient far-field radio frequency energy harvesting for passively powered sensor networks," *IEEE J. Solid-State Circuits*, vol. 43, no. 5, pp. 1287–1302, May 2008.

[11] H. Lhermet, C. Condemine, M. Plissonnier, R. Salot, P. Audebert, and M. Rosset, "Efficient power management circuit: From thermal energy harvesting to above-IC microbattery energy storage," *IEEE J. Solid-State Circuits*, vol. 43, no. 1, pp. 246–255, Jan. 2008.

[12] J.O McSpadden, et al. "Design and experiments of a high-conversion-efficiency 5.8-GHz rectenna," *IEEE MTT-S International Microwave Symp. Digest*, pp.1161–1164, 1998.

[13] J.A. Hagerty, et al. "Recycling ambient microwave energy with broadband antenna arrays," *IEEE Trans. Microwave Theory and Techn.,* pp. 1014-1024, March 2004.

[14] T. Paing, J. Shin, R. Zane, Z. Popovic, "Resistor Emulation Approach to Low-Power RF Energy Harvesting," *IEEE Trans. Power Electron.*, vol. 23, no. 3, pp1494-1501, May 2008.

[15] T. Paing, E. Falkenstein, R. Zane Z. Popovic, "Custom IC for ultra-low power RF energy harvesting," in *Proc. Applied Power Electronics Conf. (APEC)*, Washington DC, Feb. 15–19, 2009, pp.1-7.